

Surface micromachined pressure transducers

H. Guckel

Wisconsin Center for Applied Microelectronics, Department of Electrical and Computer Engineering, University of Wisconsin, Madison, WI 53706 (U.S.A.)

(Received August 10, 1990; accepted January 17, 1991)

Abstract

Typical IC processing is fundamentally two dimensional; sensors are three-dimensional structures. In surface micromachining, two-dimensional IC processing is extended to sensor structures by the addition of one or more sacrificial layers which are removed by lateral etching. The resulting sensor structures involve the substrate and one or more deposited films which form the intended micromechanical component. The concepts of this type of sensor manufacturing are readily demonstrated by considering absolute pressure transducers in some detail.

Absolute pressure transducers involve a vacuum-sealed cavity and a deformation sensing technique. The cavity is formed from the substrate and a low-pressure chemical vapor deposited polycrystalline silicon film. The mechanical properties of this film must be controlled well enough to allow the device to be designed. This implies morphological control during processing. Optimized films which do exhibit controlled compressive or tensile strains exclude oxygen or nitrogen and are therefore not modified by extended hydrofluoric acid etches. Their mechanical behavior is monitored by micromechanical test structures which measure Euler buckling and thereby determine the value of the built-in strain.

The cavity vacuum is established by reactive sealing. Long-term vacuum integrity is achieved by a low-stress silicon nitride barrier which also acts as a dielectric isolation barrier.

Sensing is accomplished via deposited polysilicon resistors. These devices behave like metal resistors in terms of their temperature coefficient of resistance and noise figure. Their piezoresistive behavior is larger than that of typical metal film structures and smaller than that of single-crystal resistors.

Pressure sensors with four diaphragms, two active and two inactive, have been constructed and optimized towards manufacturability. The measured performance is excellent and agrees with the predictions of the design algorithm.

Introduction

Pressure transducers are fundamentally pill boxes which deform geometrically due to the applied pressure or pressures which are to be measured [1, 2]. Pill box construction normally involves two separate pieces of material which are eventually joined. One of these sections is always silicon. Typically it is locally thinned by bulk micromachining via crystallographic and dopant-controlled etch stops to produce the deflecting member or diaphragm of the pill box. The remaining section is physically attached to the machined material. The use of Pyrex allows electrostatic bonding to be used for the assembly. However, it also results in a device which uses two different materials. Wafer-to-wafer bonding

produces a single material device but does require high-temperature heat cycles.

The pill box may be sealed to vacuum levels to produce an absolute pressure transducer. A device of this type requires an over-pressure stop to protect the diaphragm from deflections which exceed the fracture limit of the deformable member. Two over-pressure stops are required for a device which measures the difference between two applied pressures. This transducer, the differential pressure transducer, is therefore more complicated than the absolute sensor.

The conversion of the induced deflections to electronic signals requires a sensing scheme. The most widely used technique involves diffused or deposited resistors which are strain sensitive [3-5]. The most important argument

for this type of transduction is that of insensitivity to the parasitic elements that are typical in integrated circuits [6]. The cofabrication of sensor and amplifier is therefore not a necessity [7, 8]. The disadvantage of this scheme involves several factors [9]. Accurate resistor measurements require accurate voltage or current supplies. Since resistance values change by 1 or 2% over the operating span of the transducer, the accuracy of the measurement must exceed 0.01%. The fact that the output signal is temperature sensitive is annoying, but can be avoided by electronic means if the temperature sensitivity is known and repeatable.

An alternative to piezoresistive transduction is capacitive sensing [10-14]. In this scheme, the need for a highly accurate power supply can be lessened considerably. However, there are parasitic problems which become very important as the device size is reduced. The necessity for the cofabrication of some electronics has to be traded off against the reduction in data extraction electronics which arises from much improved temperature behavior and, of course, the reference supply issue.

A much more advanced sensing scheme involves resonating elements which are used as force transducers and change their resonance frequency with applied axial load [15-17]. Their advantages are found in their output signal: a frequency or time measurement and therefore an easily measured and digitized signal, and the need for a relatively simple driving system as well as excellent temperature stability. The disadvantages are in two main areas: cost and packaging.

A fourth transduction possibility is that of optical sensing. The potential for this technology is very large. However, cost effectiveness and survival in the very harsh environment to which sensors are subjected have yet to be demonstrated.

The goal of the work reported here is to understand surface rather than bulk micromachining techniques for sensor and actuator applications [18]. A suitable test vehicle for this purpose is the pressure transducer with known performance and market potential and, most importantly, a better than good possibility of industrial acceptance. The possible improvements involve first of all the pill box.

This structure should be made from a single material to avoid thermal mismatch and therefore internal stresses which typically lead to aging effects and hysteresis. Silicon is the material of choice. This is simply a default to practicality and offers a basis for comparison with existing devices. A second set of goals involves linear size reductions by at least a factor of ten, which force the thickness of the deflecting member of the pill box into the few micron range. This can be achieved with a bulk machined device with proper etch stops. However, the packing density will be low because etching through the wafer is involved. More serious is the lack of an overpressure stop. An alternative, wafer-to-wafer bonding and polishing, avoids the over-pressure stop issue. The required diaphragm thickness control, better than $\pm 1\%$ at 1 μm nominal thicknesses, as well as material integrity during high-temperature processing will cause difficulties for this approach. This leads to the use of deposited polysilicon film as the deflecting material by near default [19-21]. The expected nominal film thicknesses are easily achieved in this technology. Deposition uniformity can be attained in this type of process. However, there is a caveat. Normally depositions are monitored *in situ* during deposition. Polysilicon depositions are normally based on low-pressure chemical vapor processes, which are difficult if not impossible to monitor by *in situ* techniques in today's reactors. Thus, thickness control becomes a source for concern. Even more important is the fact that device production rather than device feasibility requires very tightly controlled mechanical properties for these thin films. Whether this is in fact achievable is indeed a question to which the answer is not known.

Surface micromachining implies single-sided wafer processing and insensitivity to wafer orientation. Since standard IC processing is nearly completely two dimensional and a pill box is a three-dimensional object, surface micromachining via IC processing requires lateral etching of a sacrificial layer that defines the interior of the pill box [22, 23]. Etch selectivity between the sacrificial material, the silicon substrate and the polysilicon diaphragm must be nearly infinite. The attractiveness of silicon dioxide and

hydrofluoric acid etches is set by the availability and prior art. However, since there are indications in the literature that polysilicon, especially doped polysilicon, is attacked by HF etches, concern about the feasibility arises [24]. Here it is sufficient to note that modifications in the mechanical properties of the deposited silicon film due to sacrificial layer etching would be unacceptable and, therefore, would have to be addressed during process development. A series of material science issues for which solutions are needed is thus quite evident.

The magnitude of the above problems is sufficiently significant to limit additional complications in the processing sequence. The exclusion of co-fabricated data-extraction circuitry falls into this category. The choice of the most easily implemented sensing scheme, piezoresistors, also has its origin at least in part in this line of reasoning. The implementation of resistive sensing involves several possibilities. Perhaps the most direct method is that of diffusing resistors into the polysilicon diaphragm. This approach was discarded because of leakage current problems and, more importantly, local strain variations due to the implants. A second option, dielectric isolation of the polysilicon diaphragm via a low-stress silicon nitride layer and the deposition of fully encapsulated polysilicon resistors, offered better anticipated performance and solved a second problem: a permeation barrier for gas diffusion through the diaphragm. Finally, there is the question of transducer type, absolute or differential. A differential device would of course have large application potential. However, it does require a second over-pressure stop which must be able to support rather large forces. This requires processing on highly non-planar surfaces. The absolute device, on the other hand, has to be vacuum sealed. The solution to the sealing problem appeared to be less demanding than the planarization issue [25]. The situation was compromised by selecting an absolute pressure transducer as the test vehicle and by insisting that the major processing sequences could be fully adapted to differential pressure transducer manufacture.

The thin-film material problem

Surface micromachined devices use thin films in mechanical applications. The present situation calls for two very specific films, polysilicon and silicon nitride. Both films can be produced by low-pressure chemical vapor deposition (LPCVD) techniques. Both films must be fabricated with known and controllable built-in strain, ϵ_0 ; Young's Modulus, E ; Poisson ratio, ν , and tensile strength, T . Structurally, however, the two films are quite different. Thus, polysilicon is normally but not always a polycrystalline material, whereas silicon nitride is amorphous. The two films are also very dissimilar as far as deposition conditions are concerned. Thus, polycrystalline silicon films are deposited by thermally decomposing a single gas (silane or SiH_4). A common technique for the fabrication of silicon nitride films involves a mixture of dichlorosilane, SiCl_2H_2 and ammonia, NH_3 . It is therefore not necessarily true that the end result is a silicon nitride, Si_3N_4 , film but more generally a non-stoichiometric and therefore potentially unstable phase of the form Si_xN_y .

The anticipated sensor construction insists on predetermined values of ϵ_0 , E , ν , and T . Process and equipment optimization to achieve this implies that the four quantities can be measured. This is not an easy task and is complicated further by the requirement for fast turn-around, which is needed for feedback into largely experimental procedures. This situation simplifies considerably if one realizes that a reproducible local rather than global value of the built-in strain field is a necessary condition for repeatable values of E , ν and T . Reproducibility of ϵ_0 in turn requires a polysilicon film with constant morphology. Furthermore, since single-crystal silicon has direction-dependent values of Young's modulus and the Poisson ratio, and since this dependence reflects itself into the properties of an oriented polysilicon film, a fact which is undesirable, it is necessary to produce films with randomized morphology [26].

The emphasis on film structure suggests that nucleation conditions for the film are critical. This implies that substrate preparation becomes a major issue. The required

cleaning cycles must deal with three different substrates; silicon, silicon dioxide and silicon nitride. In all cases inorganic cleaning in 180 °C sulfuric acid is followed by hydrofluoric acid etching to remove oxide layers. Immersion into ammonium hydroxide/hydrogen peroxide mixtures continues the cleaning cycle. A second HF etch prior to a final rinse is used to complete the procedure. In all cases, the purity of the chemicals is questioned. This is particularly true for the deionized water, which is not only monitored for resistivity, but also for dissolved solids and, in particular, is rejected if any bacteria count is detected. The cleaning cycle is of course followed by immediate immersion into the LPCVD reactor.

The silane reactor which is used for the work reported here is reasonably standard. Its heart is a quartz tube in a three-zone diffusion furnace which is pumped by an oversize pump. Pressure regulation is achieved by buffering the pump with nitrogen injection. The wafers are supported on a quartz boat with a 2.5 mm spacing. Dummy wafers are used to improve uniformity and all loading and unloading operations are performed with a manual cantilever system which prevents boat-to-tube contact and thereby avoids particulate pick-up. Gas injection occurs opposite to the pump stack. No diffusers or internal distributors are used. Two different gases are injected and monitored with mass-flow meters. They are purified nitrogen and VLSI grade silane. The nitrogen is only used for purging and venting. It is injected with controlled ramps to prevent particulate contamination. Silane is injected in two modes: the start or low-flow mode, which is also ramped, and the operate or high-flow mode with its ramp. Figure 1 summarizes the system.

Typical operating conditions are: start flow, 3 cm³/min for 1.7 min; high flow, 48 cm³/min; pressure, 300 mTorr; temperature, 590 °C. The growth rate will be 68 Å/min.

The reactor and its operation are not unusual. The attention to detail is: all parts of the system are always in a defined state. Thus, sections of the vacuum system are pumped, pressurized or used but never allowed to leak to air. The reactor leak rate is always monitored and special caution is used to detect internal leaks, because nitrogen as well as

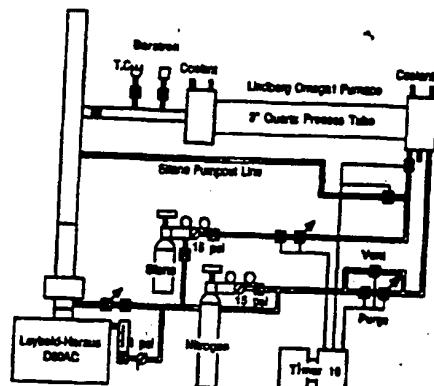


Fig. 1. Polysilicon deposition system.

ambient gases would destroy film quality if incorporated into the polysilicon film.

A finished film is inspected by optical techniques. Its surface roughness is measured and is expected to be near 8 Å r.m.s. The film is next subjected to a 48% HF bath for 24 h at room temperature. It is rinsed and its surface roughness is remeasured. If this roughness has increased, the film is rejected. This type of failure is normally due to nitrogen and/or oxygen contamination of the film and points to a reactor defect or a contaminated silane supply. A patterned polysilicon on silicon film, which is subjected to the HF etch, can help to identify the source of the problem.

The as-deposited film is in very high compression. This statement is easily verified by etching the film from the backside of the wafer and then measuring the radius of curvature of the test piece. There will be a strong tendency for it to cup up. The question now becomes one of uniformity: is the strain field changing over the wafer surface and is it changing in the direction of the film?

A nearly perfect tool to answer these questions is found by the use of mechanical test structures. The measurement technique must provide values for E , ν , or ϵ_0 [27, 28]. However, the property which is to be measured cannot be influenced by changes in the other two. It is in this sense and for several other reasons that Euler buckling is advantageous [29].

The test procedure starts with a silicon wafer which is oxidized to 1 μ m. The polysilicon film is deposited and defined with a single mask into dumbbell resistor shapes. Immersion into HF frees the resistor body but not the oversized contact pads. Mechan-

ically a clamped-clamped beam results, which for a given strain field will buckle in a direction perpendicular to the substrate if its length exceeds the critical length, which is given by

$$\epsilon_0 = \pi^2 h^2 / 3L_c^2 \quad (1)$$

where h is the thickness of the film, L_c the smallest beam length at which buckling occurs and ϵ_0 the built-in compressive strain. The theory assumes first of all that the built-in strain is uniform. This is normally not true for as-deposited structures, a fact which is readily checked by adding cantilevers to the test mask and observing their behavior. A second assumption involves the absence of any lateral forces that could cause a deflection. Typically these result from surface-tension effects during drying after rinses. They can be avoided completely by observing the test structures through a deionized water cover. In the end a valid measurement involves a situation for which 50% of the beams are buckled up and 50% down. Figure 2 is an example of a test mask.

It was stated earlier that the as-deposited film has a built-in strain field which varies

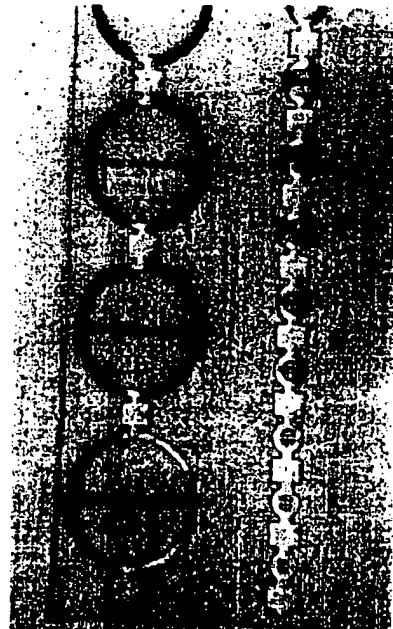
with thickness. The cure for this difficulty is normally that of annealing. A detailed study of nitrogen annealing was performed and gave somewhat surprising results. Not only did the strain field reduce, it changed sign [30]. Figure 3 shows the results.

The data in Fig. 3 led to an investigation of the film morphology via transmission electron microscopy (TEM) [31]. It was found that the as-deposited film involves two phases. The initial deposit is polycrystalline and contains crystallites which are randomly oriented and vary between 300 and 3000 Å in size. This phase is covered by an amorphous layer. During the nitrogen anneal cycle the amorphous layer converts to the crystalline phase. This involves a volume contraction which is responsible for the conversion of the compressive strain to tensile strain. Figure 4 details the film morphology.

A polysilicon film with controlled built-in strain and therefore controlled morphology may be used to measure Young's modulus. The bubble test may be used [27, 32]. In the present situation, a resonance frequency mea-



(a)



(b)

Fig. 2. Strain diagnostic test structures. (a) Doubly supported beams which have buckled. The strain is therefore compressive. (b) A ring and beam structure. This device is clamped at two points of the ring. The remaining structure is freed. The ring has contracted, which causes the beam to buckle. The strain field is therefore tensile.

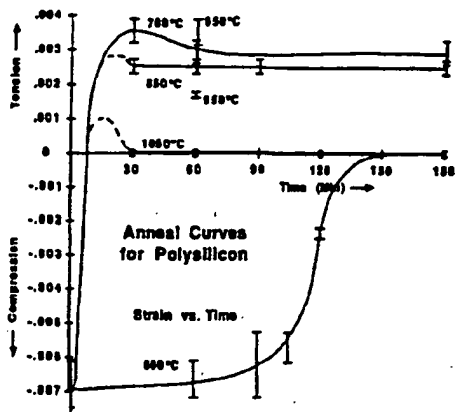


Fig. 3. The annealing behavior of fine-grained polysilicon films 2 μm thick. The horizontal axis is nitrogen anneal time in minutes. The as-deposited film is in compression. Proper annealing can produce a significant tensile field.

surement of two beams of different length is preferred because this technique fits well with other related research activities. The resonance of a clamped-clamped beam with built-in strain may be computed via perturbation calculations and is given by [33]

$$\omega_R^2 = \frac{42Eh^2}{\rho L^4} \left(1 + \frac{2L^2}{7h^2} \epsilon \right) \quad (2)$$

where ρ is the density of silicon, ϵ the total axial strain, L the beam length and h its thickness. If two beams of different length are used, Young's modulus and the built-in strain may be computed.

The emphasis in the present discussion has been on the polysilicon film. However, the anticipated pill box construction technique will also use silicon nitride films [34]. As stated earlier, this film is also an LPCVD film which is produced by reacting silane or dichlorosilane with ammonia. The stoichiometric form of this film, Si_3N_4 , is typically grown near 840 °C and involves a large tensile field. The strain values may be reduced by adjusting the gas mixtures in such a way that silicon-rich films result [35]. Very little information on strain reduction via annealing is available and, in particular, the production of zero-strain Si_3N_4 films by this technique has never been reported. This would suggest that devices which are fabricated by using this film as the pill box diaphragm will always involve built-in strains and will therefore be difficult to control from the manufacturing point of view. The somewhat less severe requirement that near-zero strain films of silicon

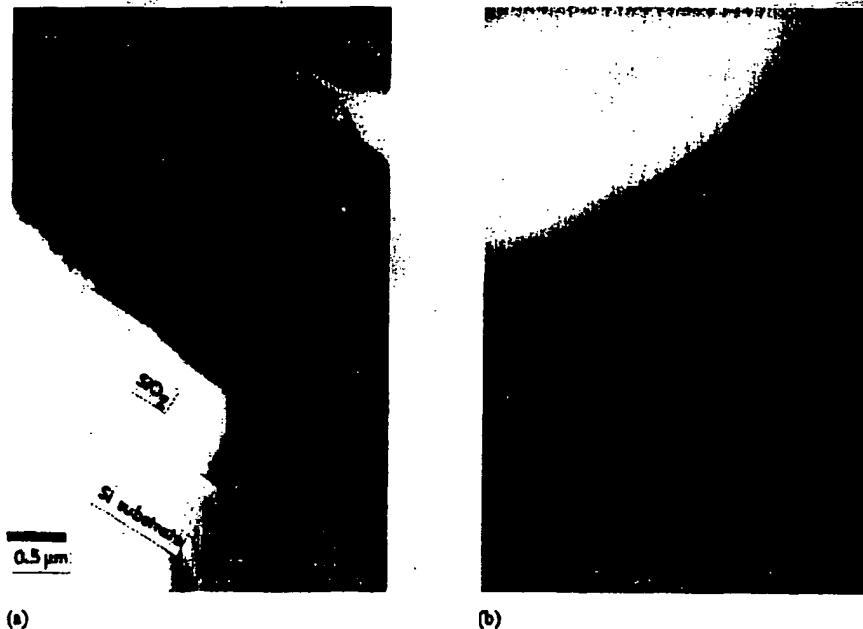


Fig. 4. (a) TEM cross section of the as-deposited polysilicon film. The two-phase film morphology is clearly visible. (b) Cross section of the annealed film. Only a single phase is present.

BEST AVAILABLE COPY

nitride act as dielectric isolation layers and do not exhibit a remarkable stiffening effect on polysilicon diaphragms is much more realistic and has in fact been found to be acceptable.

Pill box formation

It was stated earlier that the deposition rate for polysilicon as reported here is 68 Å/min. This implies that a 2 μm thick film can be grown in somewhat less than 5 h. An additional hour or so is needed for loading, flushing, venting and unloading. Films of this thickness therefore fit well into a typical working day. They also yield a processing sequence in which the planarity is not severely compromised.

It is highly desirable to fabricate diaphragms which deflect linearly with pressure. This implies that stretching effects, which are known to produce nonlinearities, must be avoided. This can be accomplished by restricting the maximum deflection of the transducer membrane to roughly 20% of the diaphragm thickness. The shape of the thin plate in this technology can be anything which can be drawn on the photomask. Thus square, rectangular and circular pill boxes have been designed and fabricated. Here the discussion will be restricted to square plate devices which typically utilize 2 μm thick polysilicon films and involve an internal pill box height of 0.75 μm . The square has a length a which is determined from the maximum pressure to be measured.

The construction technique starts with a silicon wafer of arbitrary orientation. The wafer may be doped or ion implanted if a solid ground plane is required. The material is oxidized to 200 Å and 800 Å of silicon-rich low-stress nitride is applied. Mask #1 defines the regions in which the cavities are to be located. The nitride is removed by reactive etching with CF_3O_2 , the oxide via buffered HF. A first thermal oxidation follows. The total oxide thickness is 7500 Å, which implies that roughly 3700 Å of silicon have been consumed. This first oxide is removed and the wafer is reoxidized to grow another 7500 Å of oxide. The total amount of silicon which has been oxidized is now 7500 Å. The

oxide is nearly planar with the nitride surface. Figure 5 illustrates the end result.

Mask #2 is used to pattern the silicon nitride for etch channels and polysilicon contact areas. This is demonstrated in Fig. 6. Roughly 50% of the nitride in the contact area is removed. This is adequate for highly reliable polysilicon to silicon substrate adhesion, which profits by a significant amount of solid-phase epitaxy during subsequent heat cycles. The etch channels meander and involve short straight sections. This type of layout

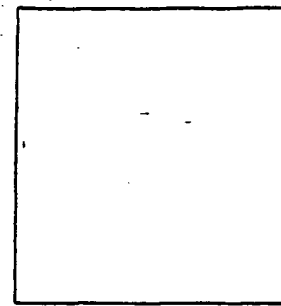


Fig. 5. Isoplanar oxide post formation.

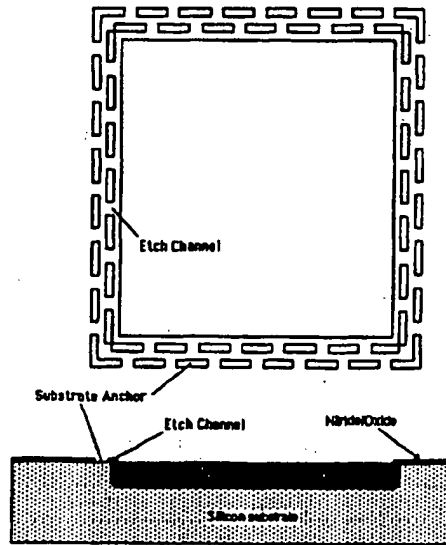


Fig. 6. Etch channel definition.

produces a stronger mechanical structure which will not easily collapse during high-temperature processing for which polysilicon can creep significantly.

The next processing step is that of polysilicon deposition. At this point there is an option. If the built-in strain is to be removed completely, a nitrogen anneal cycle at 1050 °C for 3 h is used to accomplish this. If the diaphragm is to be used with a predetermined amount of tensile strain, a modified anneal cycle may be used or subsequent heat cycles are utilized to accomplish the desired end result.

Mask #3 defines unwanted polysilicon areas. This include via cuts to the etch channels, as Fig. 7 illustrates.

The etching procedure is again reactive ion etching with NF₃ as the etch gas. The wafer is next immersed into a 1:1 mixture of VLSI grade HF and water at room temperature. Since the etch is self-limiting, over-etching is allowed. Cleaning cycles which involve hot deionized water and ammonium hydroxide-hydrogen peroxide rinses follow and normally lead to fully freed, straight plates. Larger geometries require freeze-sublimation cycles to avoid diaphragm-to-substrate sticking.

The construction technique continues with the sealing step. Ideally, this is done in an oxygen ambient at atmospheric pressure at

980 °C. The conversion of silicon produces two volumes of silicon dioxide. The etch channels will therefore close and disconnect the cavity interior from the oxygen supply. The oxygen in the cavity continues to react and produces an excellent vacuum. This procedure works quite well. However, it does result in a cavity interior that is covered by oxide. This can cause two problems: geometric distortions due to the highly compressive oxide and diaphragm-to-substrate sticking on contact. A modified sealing technique, which starts with a short oxidation and follows with a low-strain nitride deposition, completely eliminates the sticking problem. However, it does compromise the vacuum level somewhat, which is acceptable for pressure transducers but unacceptable for high-*Q* resonators that use this type of sealing. The sealing issues are still an active research topic and are continuing to receive detailed attention.

The actual design of the pill box portion of the transducer occurs in two steps: a preliminary design via explicit plate deflection theory and a refinement of the design via finite-element analysis. For a square plate which is loaded by the uniform pressure *q* the maximum deflection occurs at the plate center. It is given by

$$\omega_{\max} = \frac{0.0152qa^4(1-\nu^2)}{Eh^3} f(\epsilon_0) \quad (3)$$

where

$$f(\epsilon_0) = \left(1 + \frac{qa^2(1+\nu)\epsilon_0}{4\pi^2h^2} \right)^{-1} \quad (4)$$

Equation (4) is used with $\epsilon_0 > 0$ for tensile fields and with $\epsilon_0 < 0$ for compressive strain. It is evidently true that diaphragm design for a material with a built-in strain field is possible. In particular, built-in tensile fields can cause significant stiffening and therefore can lead to size reductions for a given load condition. On the other hand, compressive fields yield a more flexible diaphragm. However, there is a fundamental limitation; buckling can occur and is clearly evident in eqn. (4), which has a pole at

$$\epsilon_0 = \frac{-4\pi^2}{9(1+\nu)} \left(\frac{h}{a} \right)^2 \quad (5)$$

Whether one can take advantage of the built-in strain depends on process control over ϵ_0 .

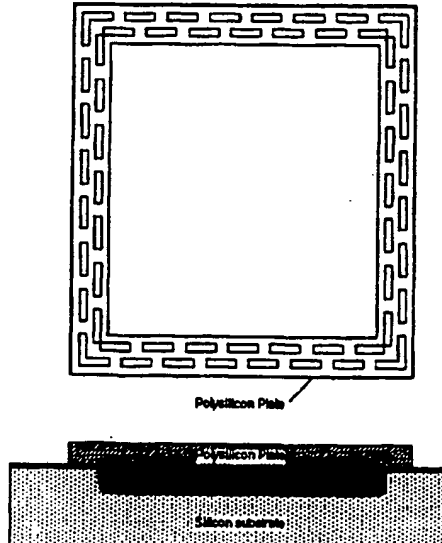


Fig. 7. Polysilicon plate definition.

and, of course, the sensitivity of device performance to process-induced strain variations. In polysilicon there is always the option of a zero built-in strain device. In silicon nitride this highly desirable feature does not exist.

Equations (3) and (4) lead to a quick estimate of the required aspect ratio by insisting that the maximum deflection, i.e., the SiO_2 gap, be a fraction of h in order to avoid non-linear plate behavior. Thus, if ηh denotes this fraction with η between 0.2 and 0.4, one obtains

$$\eta = \frac{0.0152q_{\max}a^4(1-\nu^2)}{Eh^3} \left(1 + \frac{qa^2(1+\nu)\epsilon_0}{4\pi^2h^2} \right)^{-1} \quad (6)$$

as the expression from which a/h can be computed.

The maximum bending strain for a clamped square plate occurs at the support midway between two neighboring corners. It is directed towards the plate center and is given by

$$\epsilon_x = \frac{0.3080qa^2(1-\nu^2)}{Eh^2} f(\epsilon_0) \quad (7)$$

The maximum expected strain during normal operation occurs at maximum load. It can be obtained from eqn. (7) if q is replaced by q_{\max} . This strain value is normally much smaller than the fracture strain, which is typically slightly above 1% for 2 μm thick polysilicon films. This suggests that the device has a significant over-pressure capability. The over-pressure condition will force the center portion of the diaphragm against the substrate support. This causes the pressure-sensitive area of the plate to decrease, which reduces the pressure sensitivity and therefore increases the over-pressure protection capability. The details of this calculation are quite complex and profit from finite-element analysis. Experimental studies of the over-pressure behavior are quite impressive and, for instance, result in the conclusion that a plate which is designed for touch-down at 25 psia can withstand over-pressures of 2000 psia without breakage and, more importantly, without any measurable hysteresis effects. In this case, then, smaller means better and stronger.

Resistive sensing

The previous Section dealt with the mechanical aspects of the transducer. The applied pressure-induced geometric distortions must now be converted to electronic signals. The immediate method of choice as stated earlier is that of resistive sensing. The implementation technique can follow two lines of reasoning: diffused resistors or deposited resistors. Diffused resistors, however, have very little to offer in this technology. They would have to be fabricated by cutting through the sealing nitride, which is not desirable. They would also introduce a diffusion depth dependence because they are most sensitive at the polysilicon surface. Their performance as far as temperature is concerned is not very good. The deposited resistor avoids most of these difficulties. It is the technology of choice. In order to implement this, an additional three or four masks are required.

The sealed devices are next covered with the resistor polysilicon layer. This procedure is similar to the cavity silicon deposition. A total of 4400 \AA of polysilicon is grown and implanted at 80 keV with boron. This implant establishes the sheet resistance and other properties of the sensing resistors. The next processing step involves mask #4, which provides for resistor contact regions and reduced sheet resistivity sections of the resistors via a heavy boron implant. This mask is not used in all designs. Mask #5 is used to remove unwanted resistor polysilicon. It is followed by a 1 h vacuum anneal in the silicon nitride LPCVD reactor at 835 $^{\circ}\text{C}$. 1000 \AA of strain-compensated nitride are added for complete passivation. Mask #6 is a contact mask used for metal contact opening to the resistors and ground plane. It is followed by 6800 \AA of aluminum alloy (98% Al, 1% Si, 1% Cu) applied by magnetron sputtering. A metal anneal at 480 $^{\circ}\text{C}$ in 10% hydrogen, 90% nitrogen for 30 min follows and is used prior to mask #7, the metal mask. Figure 8 illustrates the finished cross section of the device.

In order to understand the good and the bad points and the design philosophy of this device, it is useful to start with the basic properties of polysilicon as a piezoresistor [36-40].

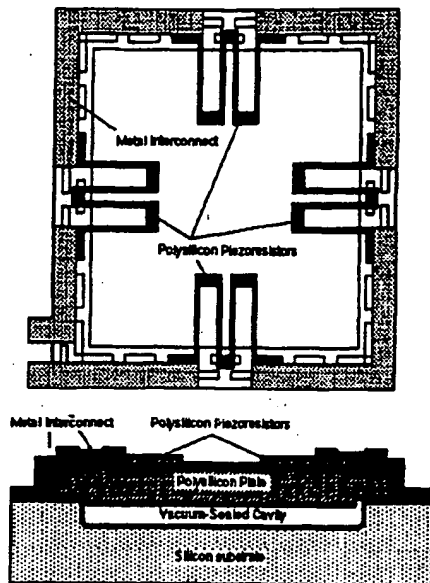


Fig. 8. Top view and cross section of planar pressure transducer.

The piezoresistive behavior of doped polysilicon can be analyzed by theoretical and experimental techniques. The theoretical calculations have been done, and will not be reported here. They indicate two things. In all cases the predicted gage factors are larger than the measured ones. Since the theory does not account for grain boundary effects, this omission is blamed for the disagreement. The calculations also predict that p-doped resistors have slightly larger gage factors than n-doped devices. Transverse and longitudinal gage factors have the expected opposite signs. The ratio of the transverse to longitudinal gage factor, which ideally should be small, again favors the p-type resistor. These theoretical conclusions were used to guide the experimental work into the boron-doped device regime.

The gage factors were measured by using a micrometer-driven cantilever. It was fabricated from the silicon substrate with a typical thickness t of 500 μm or so. If the device is b cm long and if its tip is deflected by d cm, the induced strain at some distance x from the clamped end is given by

$$\epsilon_L = 3d(b-x)/2b^3 \quad (8)$$

If a resistor is located at x and strained by ϵ_L in its longitudinal direction, the gage factor

becomes

$$G_{\text{per}} = \Delta R_L / \epsilon_L R_L \quad (9)$$

If a resistor is located at x and strained by ϵ_L in its transverse direction, the gage factor becomes

$$G_{\text{per}} = \Delta R_T / \epsilon_L R_T \quad (10)$$

where all quantities on the right of the two previous equations are measurable. Typical measured values for the silicon resistors which are used here and which are typically implanted at 80 keV into the $10^{15}/\text{cm}^2$ range are $G_{\text{per}} \approx 22.5$ and $G_{\text{per}} \approx -8.0$. The sensitivity to the implant dose is small and these values are good enough for design estimates. The temperature coefficient of the gage factor is typically near $-850 \text{ ppm}^{\circ}\text{C}$. Piezoresistive effects in polysilicon are therefore significantly below the optimum single-crystal silicon responses. However, they are very much larger than piezoresistive effects in metal films and they should really be compared to metallic film behavior and not single-crystal behavior. The argument for this is found in the following discussion.

Figure 9 illustrates the behavior of the temperature coefficient of resistance, TCR, of polysilicon resistors which have been processed as outlined here. By selecting an implant dose near $1.75 \times 10^{15}/\text{cm}^2$ at 80 keV, the TCR becomes essentially zero. The resistor would share this property with a high-quality metal resistor. Furthermore, reasonable values of positive or negative TCR are available and make the incorporation of temperature sensors and compensation networks

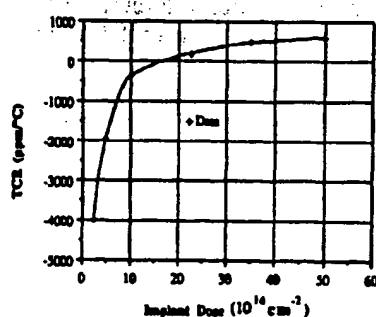


Fig. 9. Temperature behavior of boron-doped polysilicon resistors. These devices were fabricated from 4400 \AA thick polysilicon films which were blanket implanted at 80 keV for varying doses. They were then vacuum annealed at 835 $^{\circ}\text{C}$ for 90 min.

simple and implementable by the addition of one or more masks.

Figure 10 gives quite recent data on the noise figure of polysilicon resistors. The measured device exhibits only thermal noise and therefore makes significant amplification of the output signal possible. This again is something which one would expect from a metal resistor and is certainly not shared by the diffused resistors typically used for pressure transducers.

A very important issue which is related to the above topics is that of contact reliability between the polysilicon and the aluminum alloy. A resolution of this point requires extensive experimental investigation. Data collection over the last two years has provided some insight, but there is always the need for a larger data base. The conclusion now for devices which have been temperature and pressure cycled is that there is no reason for concern. The contact is stable and shows no aging effects.

The next topic involves resistor placement. In order to understand the solutions to this problem, it is well to recall that typical diaphragm sizes extend from, say, 50 to 200 μm . Resistor lengths will therefore be at most 70 μm and can be less than 20 μm with an anticipated sheet resistance near 200 Ω/\square . This implies resistor width of at best a few micrometers. Since bridge balances are required to be excellent, control of geometry during resistor manufacturing becomes a major issue.

The placement of resistors has two problem areas. A decision must be made which defines the theoretical placement. The factors which go into this are not so obvious. Thus, resistor location parallel to the clamped edge appears

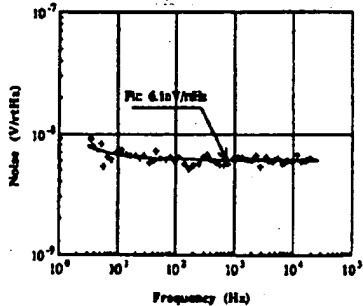


Fig. 10. Voltage noise of a boron-doped polysilicon resistor. These devices were fabricated as explained in Fig. 9.

to be attractive but really is not, because the shape of the clamped edge is not perfect. It suffers from the nemesis of isoplanar processing: the bird's beak. A resistor shape which runs perpendicular to the clamped edge is preferred. This implies that the resistor has two legs which are perpendicular to the edge and one leg, the turn-around, which is parallel to the edge. The expected resistor behavior for the two legs is given by

$$(\Delta R/R)_x = G_{par}(\epsilon_x) + G_{per}(\epsilon_y) \quad (11)$$

Maximum output occurs at positions for which the average strain field in the x -direction is a maximum. This occurs at the midpoint of the clamped edge where pressure-induced deflections cause a tensile strain. The turn-around is governed by

$$(\Delta R/R)_y = G_{per}(\epsilon_x) + G_{par}(\epsilon_y) \quad (12)$$

Since G_{per} is negative and G_{par} is positive, this term is unwanted. It can be forced to be zero by locating the turn-around at the inflection point where ϵ_x is zero. It is also possible to make the resistance of this portion of the resistor very small by raising the doping level in the turn-around. However, this can cause TCR problems as far as the terminal characteristics are concerned.

The second problem in resistor placement is that of manufacturability. Placement error due to alignment tolerances can be quite severe. This could result in a condition for which each die would have to be calibrated and trimmed. This is costly and not acceptable for this device which can be produced at low cost. Instead a resistor placement is used that is reasonably insensitive to alignment tolerances. The resistor is divided into four sections which are located at the midpoint of each clamped edge. Alignment errors, which are of course kept to a minimum, cancel to first order for this layout. The end result is the device shown in Fig. 8.

For this layout, which has the turn-around point at $x = 0.3143a$, the idealized resistance change becomes

$$\left(\frac{\Delta R}{R} \right)_x = \frac{-1.203G_{par} + 0.146G_{per}}{G_{par} + G_{per}} \left(\frac{\Delta R}{R} \right)_{0,0} \quad (13)$$

where

$$\left(\frac{\Delta R}{R}\right)_{0,0} = \frac{-0.1057(G_{par} + G_{per})(1 - \nu^2)a^2}{Eh^2} f(\epsilon_0)$$

is the sensitivity of a point resistor at the center of the plate.

The resistor which has been discussed here is forced into tension by the applied pressure. It would be advantageous to have an identical structure that produces opposite resistance changes. This can be accomplished by locating resistive structures in the center of the plate. This has been done for circular diaphragms with radial and tangential structures. Figure 11 illustrates the concept.

It is of course also true that one can take advantage of n-doped structures. This has not been investigated here. Instead, current-driven voltage dividers with one active diaphragm and one inactive diaphragm have been examined in some detail. Typical calculated data are shown in Table 1.

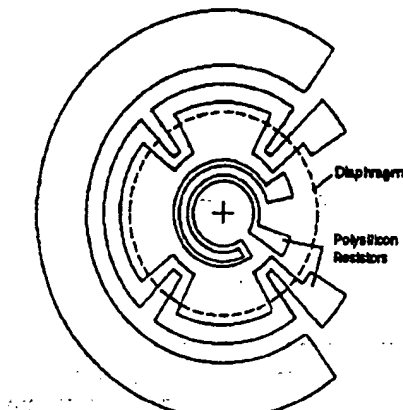


Fig. 11. Circular pressure transducer.

TABLE 1. Calculated voltage divider behavior for 2 μm polysilicon plates without built-in strain and 0.75 μm gaps

Pressure (psia)	Plate size (μm)	$\Delta R/R$ (%FS)	Sensitivity ($\mu\text{V}/\text{V}/\text{psi}$)
1	553.6	0.096	2400
1	311.3	0.303	758
10	175.1	0.959	240
100	98.4	3.03	75.8
1000	55.4	9.59	24.0

Transducer implementation

In the previous Section the interplay between resistive sensing and pill box design and fabrication was examined. The implication of this discussion is that there is a single sensing resistor per diaphragm. Furthermore, since the manufacturing and performance issues which are of interest here are adequately answered by the availability of a single resistor type rather than the customary positive and negative approach, the implementation of a bridge circuit can at best involve two pressure-sensitive diaphragms. The transducer then takes the form of two active resistors on two separate diaphragms and two inactive resistors on their respective diaphragms. Since bridge balance in the absence of applied pressure is a very serious issue as far as data extraction and compensation are concerned, a lay-out which is completely symmetrical is preferred. This is illustrated in Fig. 12.

Cost effective packaging for this type of a device can take advantage of the small sizes involved. Thus, in an application area which requires 25 psia, 250 psia, and 600 psia devices, a 80 \times 80 mil die is used which contains the three pressure ranges and therefore involves only a single packaging effort. Figure 13 illustrates the concept.

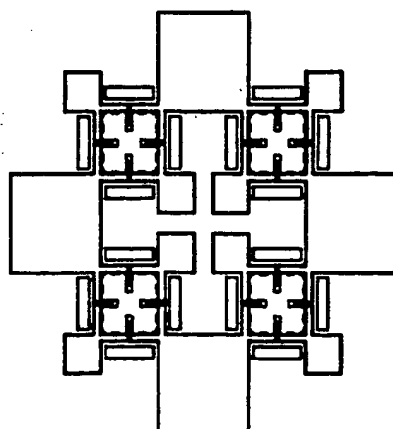


Fig. 12. Half-active full-bridge layout. The bridge-type transducer is constructed from two active or deflecting diaphragms and two diaphragms which retain the oxide post.

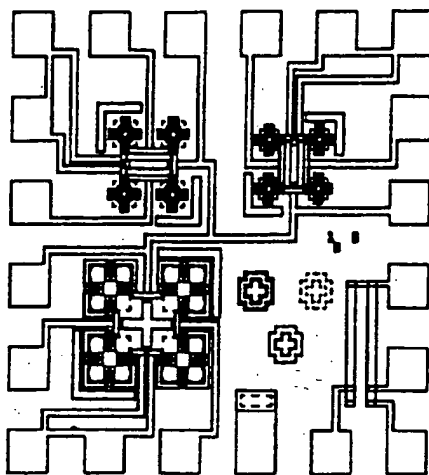


Fig. 13. Pressure transducer with three pressure ranges.

The size advantages also reflect themselves in another area. A 10×10 array of identical transducers is in the design stage. The purpose here is signal averaging, which lessens the need for calibration and contributes a very small cost increase to the packaged unit. A fault redundant design has also been examined. However, the need for this approach has been reduced considerably by field test data which indicate that diaphragm failure is an extremely rare occurrence.

Finally, a word of caution. The small size also has a disadvantage in that power dissipation must be restricted. Thus, devices with poor heat sinks are only operated to a few milliwatts. Devices which are in oil-filled packages minimize this problem and can be operated with high bridge voltages.

Conclusions

The device discussed here is now in its third iteration. Extensive tests have been done on version #2. The test data, which are unfortunately company confidential, yield the conclusion that the devices perform very well and that they are also fully designable. Perhaps the best feature is the absence of hysteresis after temperature over-pressure tests of many cycles. The confidence limit with a custom electronic interface results in the conclusion that on a 25 psia device, repeatability to 0.001% of full scale has been achieved for operating temperatures from -55 to 125°C .

Extension to higher temperatures is possible but requires a metallurgy change. Device-to-device tracking is quite good and the manufacturing yield is very high, with packing densities approaching 20 000 devices per 3" wafer for simple devices. The devices do have a drawback. A linearity of 0.2% FS is quite easily obtainable. However, better linearities will require thicker plates to avoid stretching and additional improvements would result from a reduced bird's beak. Since there are applications for which repeatability is the main issue and linearity a secondary consideration, a more careful examination of this topic has been postponed.

The overall progress for this type of device has been sufficiently encouraging for realistic differential pressure transducers to be considered. The second over-pressure stop issue has recently been solved and designs for 1" water transducers with very significant over-pressure capability will be reported on soon.

References

- 1 R. S. Medlock, Sensors for mechanical properties, *J. Phys. E: Sci. Instrum.*, 16 (1983) 964-972.
- 2 J. Bryzek, Modeling performance of piezoresistive pressure sensors, *Proc. 3rd Int. Conf. Solid-State Sensors and Actuators (Transducers '85)*, Philadelphia, PA, U.S.A., June 11-14, 1985, pp. 168-173.
- 3 E. R. Peake, A. R. Zias and J. V. Egan, Solid state digital pressure transducer, *IEEE Trans. Electron Devices*, ED-16 (1969) 870-876.
- 4 W. H. Ko, J. Hynacek and S. F. Boettcher, Development of a miniature pressure transducer for biomedical applications, *IEEE Trans. Electron Devices*, ED-26 (1979) 1896-1905.
- 5 M. Esashi, H. Komatsu, T. Matsuo, M. Takahashi, T. Takishima, K. Imabayashi and H. Ozawa, Fabrication of catheter-tip and sidewall miniature pressure sensors, *IEEE Trans. Electron Devices*, ED-29 (1982) 57-63.
- 6 M. Shimazoe, Y. Matsupka, A. Yasukawa and M. Tanabe, A special silicon diaphragm pressure sensor with high output and high accuracy, *Sensors and Actuators*, 2 (1982) 275-282.
- 7 K. Yamada, M. Nishihara, R. Kanazawa and R. Koyabashi, A piezoresistive integrated pressure sensor, *Sensors and Actuators*, 4 (1983) 63-69.
- 8 S. Sugiyama, M. Takigawa and I. Igaraishi, Integrated piezoresistive pressure sensor with both voltage and frequency output, *Sensors and Actuators*, 4 (1983) 113-120.
- 9 M. Esashi, H. Komatsu and T. Matsuo, Biomedical pressure sensor using buried piezoresistors, *Sensors and Actuators*, 4 (1983) 537-544.

10 C. S. Sander, J. W. Knutti and J. D. Meindl, A monolithic capacitive pressure sensor with pulse-period output, *IEEE Trans. Electron Devices, ED-27* (1980) 97-930.

11 Y. S. Lee and K. D. Wise, A batch-fabricated silicon capacitive pressure transducer with low temperature sensitivity, *IEEE Trans. Electron Devices, ED-29* (1982) 42-48.

12 Wen H. Ko, M. H. Bao and Y. D. Hong, A high sensitivity integrated circuit capacitive pressure transducer, *IEEE Trans. Electron Devices, ED-29* (1982) 48-56.

13 C. D. Fung and W. H. Ko, Miniature capacitive pressure transducers, *Sensors and Actuators*, 2 (1982) 321-326.

14 W. H. Ko, B. X. Shao, C. D. Fung, W. J. Shen and G. J. Yeh, Capacitive pressure transducers with integrated circuits, *Sensors and Actuators*, 4 (1983) 403-411.

15 K. Ikeda, H. Kuwayama, T. Kobayashi, T. Watanabe, T. Nishikawa and T. Yoshida, Silicon pressure sensor with resonant strain gauges built into diaphragm, *Tech. Digest, 7th Sensor Symp., Shigaku Kaikan, Tokyo, Japan, May 1988*, pp. 55-58.

16 K. Ikeda, H. Kuwayama, T. Kobayashi, T. Watanabe, T. Nishikawa and T. Yoshida, Three-dimensional micromachining of silicon resonant strain gauge, *Tech. Digest, 7th Sensor Symp., Shigaku Kaikan, Tokyo, Japan, May 1988*, pp. 193-196.

17 H. Guckel, J. J. Sniegowski and T. R. Christenson, Construction and performance characteristics of polysilicon resonating beam force transducers, *Third Toyota Conf., Nisrin, Aichi, Japan, Oct. 1989*, pp. 23 (1-10).

18 D. W. Burns, Micromechanics of integrated sensors and the planar processed pressure transducer, *Ph.D. Thesis, University of Wisconsin-Madison*, May 1988.

19 H. Guckel, D. W. Burns, C. R. Rutigliano, D. K. Showers and J. Uglow, Fine grained polysilicon and its application to planar pressure transducers, *Proc. 6th Int. Conf. Solid-State Sensors and Actuators (Transducers '87), Tokyo, Japan, June 2-5, 1987*, pp. 277-282.

20 R. T. Howe and R. S. Muller, Integrated resonant-microbridge vapor sensor, *IEDM 1984*, pp. 213-216.

21 R. T. Howe and R. S. Muller, Resonant-microbridge vapor sensor, *IEEE Trans. Electron Devices, ED-33* (1986) 499-506.

22 T. Randazzo, An investigation into the use of polysilicon as a sensor material, *Master's Report, University of Wisconsin-Madison*, Aug. 1983.

23 R. T. Howe and R. S. Muller, Polycrystalline silicon micromechanical beams, *J. Electrochem. Soc., 130* (1983) 1420-1423.

24 T. I. Kamins, M. M. Mandurah and K. C. Saraswat, Structure and stability of low pressure chemically vapor-deposited films, *J. Electrochem. Soc., 125* (1978) 927-931.

25 H. Guckel and D. W. Burns, Planar processed polysilicon sealed cavities for micromechanical sensors, *IEDM 1984, San Francisco, CA, U.S.A.*, pp. 223-225.

26 H. Guckel, D. W. Burns, H. A. C. Tilmans, D. W. DeRoo and C. R. Rutigliano, Mechanical properties of fine grained polysilicon - the repeatability issue, *1988 Solid-State Sensor and Actuator Workshop, Hilton Head Island, SC, U.S.A., June 6-9, 1988*.

27 S. D. Senturia, Microfabricated structures for the measurement of mechanical properties and adhesion of thin films, *Proc. 4th Int. Conf. Solid-State Sensors and Actuators (Transducers '87), Tokyo, Japan, June 2-5, 1987*, pp. 11-16.

28 M. Mehregany, M. G. Allen and S. D. Senturia, The use of micromachined structures for the measurement of mechanical properties and adhesion of thin films, *IEEE Solid State Sensor Workshop, Hilton Head Island, SC, U.S.A., June 2-5, 1986*.

29 H. Guckel, T. Randazzo and D. W. Burns, A simple technique for the determination of mechanical strain in thin films with applications to polysilicon, *J. Appl. Phys.*, 57 (1983) 1671-1675.

30 H. Guckel, D. W. Burns, C. G. Visser, H. A. C. Tilmans and D. DeRoo, Fine-grained polysilicon films with built-in tensile strain, *IEEE Trans. Electron Devices, ED-35* (1988) 800-801.

31 H. Guckel, J. J. Sniegowski, T. R. Christenson and F. Raissi, The application of fine-grained, tensile polysilicon to mechanically resonant transducers, *Sensors and Actuators*, A21-A23 (1990) 346-351.

32 O. Tabata, K. Kawahata, S. Sugiyama and I. Igarashi, Mechanical property measurements of thin films using load-deflection of composite rectangular membranes, *Sensors and Actuators*, 20 (1989) 135-141.

33 J. J. Sniegowski, H. Guckel and T. R. Christenson, Performance characteristics of second generation polysilicon resonating beam force transducers, *IEEE Solid State Sensor and Actuator Workshop, Hilton Head Island, SC, U.S.A., June 4-7, 1990*.

34 S. Sugiyama, T. Suzuki, K. Kawahata, K. Shimaoka, M. Takigawa and I. Igarashi, Micro-diaphragm pressure sensor, *IEDM 1986, Los Angeles, CA, U.S.A.*, pp. 184-187.

35 H. Guckel, D. K. Showers, D. W. Burns, C. R. Rutigliano and C. G. Nester, Deposition techniques and properties of strain compensated LPCVD silicon nitride films, *IEEE Solid State Sensor Workshop, Hilton Head Island, SC, U.S.A., June 2-5, 1986*.

36 Y. Onuma and K. Sekiya, Piezoresistive properties of polycrystalline silicon thin films, *Jpn. J. Appl. Phys.*, 11 (1972) 20-23.

37 J. Y. W. Seto, Piezoresistive properties of polycrystalline silicon, *J. Appl. Phys.*, 47 (1976) 4780-4783.

38 S. Nishida, M. Konagai and K. Takahashi, Seebeck and piezoresistance effects in amorphous-microcrystalline mixed-phase silicon films and applications to power sensors and strain gauges, *Thin Solid Films*, 112 (1984) 7-16.

39 O. Dassel, Longitudinal and transverse gauge factors of polycrystalline strain gauges, *Sensors and Actuators*, 6 (1984) 169-179.

40 E. Obermeier, P. Kopystynski and R. Niebl, Characteristics of polysilicon layers and their application in sensors, *IEEE Solid State Sensor Workshop, Hilton Head Island, SC, U.S.A., June 2-5, 1986*.